Open Access | Rapid and quality publishing

International Journal of
Electrical and Electronics Research (IJEER)
Research Article | Volume 14, Issue 2 | Pages 641-652 | e-ISSN: 2347-470X

A Novel LSTM-Enhanced TBA-IUKF Framework with Adaptive Node Selection for Energy-Efficient Target Tracking in Wireless Sensor Networks

Mohammed Aboud Kadhim[1], Ali Y. Jaber[2], and Zeyid T. Ibraheem[3]

[1,2]Polytechnic College for Engineering, Middle Technical University, Baghdad, Iraq
[3]College of Engineering, University of Information Technology and Communications, Baghdad, Iraq

***Correspondence:** *Mohammed Aboud Kadhim, mohammed_aboud@mtu.edu.iq*

ABSTRACT- This paper presents TBA-IUKF-DL, a rigorously formulated hybrid framework that couples an Iterated Unscented Kalman Filter (IUKF) with a dual-layer Long Short-Term Memory (LSTM) residual-correction network and the Tiger Beetle Algorithm (TBA) for energy-efficient target tracking in resource-constrained Wireless Sensor Networks (WSNs). Unlike existing LSTM-Kalman hybrids that treat neural correction as a decoupled post-processor, the proposed framework establishes a principled three-way coupling: (i) the IUKF executes iterative sigma-point updates whose convergence is formally proved via Lyapunov stability analysis; (ii) a dual-layer LSTM with 64 hidden units per layer, tanh cell activations, and dropout regularization ($p = 0.2$) is trained with Adam optimization ($\eta = 0.001$, MSE loss) to predict systematic residuals from unmodelled dynamics; and (iii) TBA—a three-phase swarm intelligence method modelling tiger-beetle predation—maximizes a composite information-energy utility function to identify the minimal active node subset at each step. Validation over 100 Monte Carlo trials in MATLAB R2023b on a 50-node, 100×100 m² WSN demonstrates RMSE = 0.726 ± 0.098 m, a 23.7% reduction over TBA-IUKF ($p < 0.001$), 31.4% energy saving, and 45.2% lifetime extension. The contribution of every component and environmental robustness is confirmed by performing an ablation study and sensitivity analysis respectively.

Keywords: WSN, Target Tracking, IUKF, LSTM, Tiger Beetle Algorithm, Adaptive Node Selection, Energy Efficiency, Monte Carlo Validation.

ARTICLE INFORMATION

Author(s): Mohammed Aboud Kadhim, Ali Y. Jaber, and Zeyid T. Ibraheem;

Received: 17/02/26; **Accepted**: 24/05/26; **Published**: 30/06/26;
E- ISSN: 2347-470X;
Paper Id: IJEER 1702B10;
Citation: 10.37391/ijeer.140239
Webpage-link:
https://ijeer.forexjournal.co.in/archive/volume-14/ijeer-140239.html

Publisher's Note: FOREX Publication stays neutral with regard to jurisdictional claims in Published maps and institutional affiliations.

1. INTRODUCTION

The contribution of every component and environmental robustness is confirmed by performing an ablation study and sensitivity analysis respectively. Wireless Sensor Networks (WSNs) serve as the backbone of many modern cyber-physical infrastructures [1], with applications in environmental monitoring, industrial process control, and military perimeter surveillance. Target tracking, the task of estimating the kinematic state of a moving object from spatially-distributed, noisy, range measurements is a necessary and computationally-intense procedure in this setting. By far the most limiting resource for WSNs is energy (every transmission, after all, has a cost in terms of drawing on a limited battery reserve) and the first and still most influential energy model in the area is that of Heinzelman et al. [2] found that communications largely exceeded the energy consumed by computations in WSN deployments. Therefore, both tracking accuracy and network lifetime need to be attained through principled co-optimization of the estimator and the node activation policy. Standard solution to the nonlinear state estimation in WSNs is classical Bayesian filters. The Unscented Kalman Filter (UKF) proposed by Julier and Uhlmann [3] avoids the linearization bias of the Extended Kalman Filter (EKF) using a derivative-free sigma-point approximation. The Iterated Unscented Kalman Filter (IUKF) [4], which was targeted for the passive target tracking problem, improves upon UKF through iterating on the sigma-point update step using a fixed-point iteration, making IUKF a better approximation of the maximum-a-posteriori estimate for moderately nonlinear measurement functions. The core accuracy–lifetime trade-off is not addressed by either of those classical filters, primarily because neither includes energy-aware node scheduling as part of their filtering function. KalmanNet [5] is a representative deep learning paradigm based on the model which shows that recurrent neural network modules placed on them from Kalman filter flow can help to improve the robustness of estimation in the presence of partially known dynamics. Fundamental meta-heuristic methods to WSN routing and node scheduling for energy efficiency, such as the Snake Optimizer [6], the Grey Wolf Optimizer [7], or the Dwarf Mongoose Optimization algorithm [8], have also been employed in an independent fashion with respect to the state uncertainty of the filter policy. The authors Song et al recently proposed a new method, based on long-short term memory (LSTM) followed by a single residual correction, for tracking. [9] Appropriately reducing RMSE for the radar tracking task by using LSTM models in place of the noise distributions, and Peng et al. In [10], convolutional bi-directional LSTM combined with EKF to track maneuvering WSN. Energy-aware adaptive node scheduling does not integrate into any of these methods. Here, we introduce TBA-IUKF-DL to fill these gaps, a principled three-component integration. A new addition is the Tiger Beetle Algorithm, which generalizes the Dwarf Mongoose Optimization method by Agushaka et al. Fig. [8]—is rewritten for binary nodes through a formally derived information-energy utility function. It uses a Lyapunov stability proof to prove per-iteration convergence of the IUKF update in the WSN measurement framework. Details such as the architecture for the LSTM, training objective and implementation for the protocol are specified in full and mapped to the energy-constrained multi-node WSN context as extensions of the KalmanNet paradigm [5]. The major contributions are: (1) complete formulation of TBA for joint selection of optimal nodes and guidance of LSTM hyperparameter, distinctly separating TBA-IUKF-DL from other LSTM-Kalman hybrids [5, 9, 10]; (2) Lyapunov stability proof for IUKF iterative update in WSN setups, generalization of Zhan and Wan [4]; (3) specification of complete LSTM architecture over Kalman Net paradigm [5] for energy-constrained WSN deployment; (4) 100 Monte Carlo trials, ablation and sensitivity analysis; (5) 23.7% reduction in RMSE, 31.4% in energy usage, and 45.2% in lifetime improvement over TBA-IUKF ($p < 0.001$).

2. LITERATURE REVIEW AND RELATED WORK

2.1. Target Tracking in WSNs

The WSN target tracking problem has been received sustained attention since the original survey article on deployment by Akyildiz et al. [1] and the energy model of Heinzelman and Chandrakasan. Khiadani and Hendessi introduced an energy-prediction-based tracking protocol based on a standard Kalman Filter in a work [11] with a forced handoff scheduling and showed that prediction-based node activation can reduce energy while maintaining the tracking quality. Tang et al. Stochastic Roundedness for Target Tracking in Distributed UKF Underwater WSNs with Fading Channels for, where and on the energy–accuracy trade-off of the communication-constrained deployment. Peng et al. Yukhymenko et al. in [10] presented a convolutional bi-directional LSTM model appended with extended Kalman filter (EKF) for maneuvering wireless sensor network (WSN) target tracking, demonstrating reduced RMSE compared to classical EKF but not energy-aware node scheduling.

2.2.Kalman Filter Variants

It was first introduced by Julier and Uhlmann [3] as a derivative-free method of extending EKF to nonlinear states. Meanwhile, Zhan and Wan [4] proposed the IUKF for just passive target tracking (see [5] for derivation) by iterating the sigma-point update, allowing one to obtain a closer maximum-a-posteriori approximation, but still without formal consideration of WSN energy constraints, or Lyapunov convergence analysis in the measurement-constrained setting. Arasaratnam and Haykin's cubature Kalman filter [13] offer a different third order approximation but does not build in iterative refinement or energy aware scheduling. Revach et al. The works described in [5] proposed KalmanNet, learning the Kalman gain through a recurrent neural network that works with dynamics partially known via a flat detached observation, illustrating that model-based deep learning gives performance beyond both fully model-based and fully data driven estimators. The proposed approach, namely TBA-IUKF-DL, generalizes these works by providing a formal Lyapunov convergence proof of the iterative IUKF update in WSN settings and a LSTM correction plus energy-aware node scheduling.

2.3. Deep Learning for Tracking

Song et al. [9] replaced the process model and noise distributions in a Kalman filter with LSTM networks for radar maneuvering target tracking, demonstrating consistent RMSE improvement over standard KF and EKF variants. Peng et al. [10] applied a convolutional bi-directional LSTM-EKF to WSN maneuvering targets, showing that the BiLSTM contextual representation improves tracking in the presence of noise. Buchnik et al. [14] extended KalmanNet to high-dimensional signal spaces through a learned latent representation, demonstrating improved accuracy and reduced latency over both model-based and fully data-driven baselines. The LSTM cell formulation of Hochreiter and Schmidhuber [15] provides the fundamental architecture used in all these works. A critical gap shared across all reviewed deep-learning-based tracking methods is the absence of formal Lyapunov convergence analysis and energy-aware node scheduling—both of which TBA-IUKF-DL provides.

2.4. Meta-Heuristic Optimisation for WSNs

Hashim and Hussien [6] proposed the Snake Optimizer, a biologically inspired metaheuristic that has been applied to WSN coverage and routing optimization. Mirjalili et al. [7] introduced the Grey Wolf Optimizer, which has been widely applied to WSN clustering and lifetime maximization. Agushaka et al. [8] proposed the Dwarf Mongoose Optimization algorithm, demonstrating competitive performance on continuous and discrete engineering design problems. The improved version of this algorithm [16] further enhances exploration through a modified alpha-selection mechanism. Kennedy and Eberhart's Particle Swarm Optimization [17] remain a widely used baseline for WSN node scheduling problems. None of the reviewed meta-heuristic approaches formally couple node selection with the filter's instantaneous predicted covariance through an information-theoretic utility function, which is the key structural innovation of TBA-IUKF-DL.

2.5. Positioning of the Proposed Work

Table 1 summarizes key methodological differences. The proposed framework is uniquely characterized by: iterative nonlinear estimation (IUKF [4]), formally specified LSTM correction (extending KalmanNet [5] and Song et al. [9]), TBA-based adaptive node selection (extending Dwarf

Mongoose [8, 16]), energy optimization (extending [11, 12]), and Lyapunov convergence proof. None of the reviewed work incorporates all the five attributes together.

Table 1. Methodological comparison. All citations follow order of first appearance.

Method	Filter	DL Module	Node Sel.	Energy	Conv. Proof	MC Valid.
Song et al. [9]	KF	LSTM	No	No	No	No
Peng et al. [10]	EKF	BiLSTM	No	No	No	Partial
Revach et al. [5]	KF	RNN	No	No	No	No
Buchnik et al. [14]	KF	Latent NN	No	No	No	No
Khiadani & Hendessi [11]	KF	None	KF-pred	Yes	No	Yes
Tang et al. [12]	UKF	None	No	Partial	Partial	No
Proposed TBA-IUKF-DL	**IUKF (J=5)**	**LSTM (×2)**	**TBA**	**Yes**	**Yes**	**Yes (100)**

3. SYSTEM MODEL AND PROBLEM FORMULATION

3.1. Network and State Model

Suppose that we have a WSN having the number of sensor nodes N = 50 distributed uniformly at random into A = [0, 100]×[0, 100] m². Node $i \in \{1, \ldots, N\}$ has known position s_i and initial energy Ei(0) = E0 = 2 J. A single target is tracked over T = 200 steps with Δt = 0.5 s. The 4D state vector is:

$$xk = [xk, yk, \dot{x}k, \dot{y}k]^{\mathrm{T}} \in \mathbb{R}^4 \quad (1)$$

The constant-velocity transition model is:

$$xk = Fxk - 1 + wk - 1, \;\; wk - 1 \sim N(0, Q) \quad (2)$$

$$F = \big[[1,0,\Delta t,0],[0,1,0,\Delta t],[0,0,1,0],[0,0,0,1]\big] \quad (3)$$

$$Q = q \bullet \left[\left[\frac{\Delta t^3}{3{,}0}, \frac{\Delta t^2}{2{,}0}\right], \left[0, \frac{\Delta t^3}{3{,}0}, \frac{\Delta t^2}{2}\right], \left[\frac{\Delta t^2}{2{,}0}, \Delta t, 0\right], \left[0, \frac{\Delta t^2}{2{,}0}, \Delta t\right]\right] \quad (4)$$

Where q = 0.1 m²/s³. The simulated trajectory uses a non-homogeneous motion model (constant velocity segments, constant turns at ω = 3 °/step, stochastic acceleration bursts) that is explicitly non-CV, with residuals for correction by the LSTM.

3.2. Distance-Dependent Measurement Model

Each active node $i \in$ Sk provides a range measurement:

$$zik = hi(xk) + vik, hi(xk) = \sqrt{[(xk - si, x)^2 + (yk - si, y)^2]} \quad (5)$$

$$Rik = \sigma^{02} + \sigma d^2 \bullet [hi(xk)]^2 \quad (6)$$

With σ_0^2 = 0.25 m² and σd² = 0.001. This distance-dependent noise model captures the physical degradation of measurement quality with range, motivating the information-gain term in the TBA fitness function.

3.3. Energy Consumption and Problem Formulation

The first-order radio energy model [2, 18] governs node consumption. For packet length L = 2000 bits over distance *di*:

$$Eitx = Eelec \bullet L + \varepsilon fs \bullet L \bullet di^2 \quad (transmission) \quad (7)$$

$$Eirx = Eelec \bullet L \quad (reception) \quad (8)$$

With Eelec = 50 nJ/bit and εfs = 10 pJ/bit/m². Node *i* is deactivated when Ei(k) < Eth = 0.05J. The joint tracking-energy optimization problem at step *k* is:

$$min_{Sk}\, Jk = \alpha \bullet E[\|xk - \hat{x}k\|^2] + \beta \bullet \Sigma_i \in SkEitx \quad (9)$$

$$s.t.: |Sk| \leq Mmax = 8, Ei(k) \geq Eth \forall i \in Sk, Ei(k+1) = Ei(k) - Eitx$$

Where α=0.6 and β=0.4. This is NP-hard (combinatorial submodular maximization), motivating the TBA-based approximate solver. All symbols are collected in *table 2*.

Table 2. Notation and parameter definitions.

Symbol	Definition	Value / Unit
N	Number of sensor nodes	50
T	Total time steps	200
Δt	Sampling interval	0.5 s
L	Field side length	100 m
xk	State $[x,y,\dot{x},\dot{y}]^{\mathrm{T}}$	$\mathbb{R}^4$
F	State transition matrix	4×4
Q	Process noise covariance	4×4, q=0.1 m²/s³
hi(xk)	Range measurement of node *i*	Euclidean dist.
Rik	Meas. noise variance (dist.-dep.)	σ_0^2+σd²·di²
Sk	Active node subset at time k	|Sk|≤Mmax=8
E0	Initial node energy	2 J
Eth	Deactivation threshold	0.05 J
α, β	Accuracy/energy weighting	0.6, 0.4
J	IUKF iteration count	5
H	LSTM hidden units/layer	64
Np	TBA population size	20
Ttba	TBA max iterations/step	50
γpen	TBA cardinality penalty	10
MC	Monte Carlo trials	100

FOREX Publication
Open Access | Rapid and quality publishing
International Journal of
Electrical and Electronics Research (IJEER)
Research Article | Volume 14, Issue 2 | Pages 641-652 | e-ISSN: 2347-470X

4. PROPOSED TBA-IUKF-DL FRAMEWORK

The TBA-IUKF-DL framework integrates three tightly coupled components per time step: (1) TBA selects the energy-optimal active node subset Sk using the current predicted covariance; (2) IUKF executes J=5 iterative sigma-point updates using measurements from Sk; and (3) the LSTM predicts and corrects systematic residuals, feeding an improved state estimate back to TBA at the next step through the updated covariance.

4.1. IUKF with Lyapunov Convergence Proof

4.1.1. Prediction Step

$$\hat{x}k|k-1 = F \bullet \hat{x}k-1|k-1 \quad (10)$$

$$Pk|k-1 = F \bullet Pk-1|k-1 \bullet F^{\mathrm{T}} + Q \quad (11)$$

4.1.2. Sigma-Point Generation (2n+1 = 9 points, n = 4)

$$\chi 0 = \hat{x}k|k-1 \quad (12)$$

$$\chi i = \hat{x}k|k-1 + (\sqrt{[(n+\lambda)Pk|k-1]})_{\mathrm{i}}, i = 1,\dots,n \quad (13)$$

$$\chi i + n = \hat{x}k|k-1 - (\sqrt{[(n+\lambda)Pk|k-1]})_{\mathrm{i}}, i = 1,\dots,n \quad (14)$$

$$W0(m) = \frac{\lambda}{n+\lambda}, Wi(m) = \frac{1}{[2(n+\lambda)]}, \lambda = \alpha^2(n+\kappa) - n \quad (15)$$

$$W0(c) = W0(m) + (1 - \alpha^2 + \beta_U KF), Wi(c) = Wi(m) \quad (16)$$

$$with\ \alpha = 10^{-3}, \kappa = 0, \beta_{UKF} = 2.$$

4.1.3. Iterative Measurement Update (j = 1, …, J = 5)

$$Zi,k(j) = h\big(\chi i(j-1)\big), i = 0,\dots,2n \quad (17)$$

$$\hat{z}k(j) = \Sigma_{\mathrm{i}} Wi(m) Zi,k(j) \quad (18)$$

$$Pzz(j) = Rk + \Sigma_{\mathrm{i}} Wi(c)[Zi,k(j) - \hat{z}k(j)][Zi,k(j) - \hat{z}k(j)]^{\mathrm{T}} \quad (19)$$

$$Pxz(j) = \Sigma_{\mathrm{i}} Wi(c)[\chi i(j) - \hat{x}k|k-1][Zi,k(j) - \hat{z}k(j)]^{\mathrm{T}} \quad (20)$$

$$Kk(j) = Pxz(j) \bullet [Pzz(j)]^{-1} \quad (21)$$

$$\hat{x}k|k(j) = \hat{x}k|k-1 + Kk(j) \bullet \big(zk - \hat{z}k(j)\big) \quad (22)$$

$$Pk|k(j) = Pk|k-1 - Kk(j) \bullet Pzz(j) \bullet [Kk(j)]^{\mathrm{T}} \quad (23)$$

4.1.4. Lyapunov Convergence Proof

Proposition 1: Under the assumption that h is twice continuously differentiable and $\|Hk\| \le Hmax < \infty, V(j) = trace(Pk|k(j))$ is monotonically non-increasing per iteration.

Proof: From *eq. (23)*:

$$V(j) = trace(Pk|k-1) - trace(Kk(j) \bullet Pzz(j) \bullet [Kk(j)]^{\mathrm{T}}) \le V(j-1) \quad (24)$$

Since trace$(K \bullet Pzz \bullet K^{\mathrm{T}}) \ge 0$ for positive definite Pzz (guaranteed by the addition of positive-definite Rk in *eq. 19*).

The contraction ratio is:

$$\gamma k(j) = \|I - Kk(j) \bullet Hk\|F^2, \gamma k(j) < 1 \Leftrightarrow Kk(j)Hk\ is\ positive\ definite \quad (25)$$

$$V(j) \le \gamma k(j) \bullet V(j-1) \le \gamma k(j)^j \bullet trace(Pk|k-1) \quad (26)$$

Since $0 < \gamma k(j) < 1$under the stated conditions, V(j) converges geometrically to a fixed point. In practice J=5 iterations are sufficient (verified in simulation).

4.2. LSTM Residual Correction Network

4.2.1. Motivation

Motivation: The CV model produces systematic residuals $\varepsilon k = xk - \hat{x}k \mid kIUKF$ during turns and bursts. An LSTM [15] is appropriate to model these temporally correlated patterns, as shown for tracking problems by Revach et al.) [5] and Song et al. [9].

4.2.2. Architecture

Input layer: $u_k = [\hat{x}_{k-L:k}; z_{k-L:k}] \in \mathbb{R}^{6\times L}, L = 10$steps

LSTM Layer1: 64 hidden units, tanh cell activation, sigmoid gates, dropout $p_d = 0.2$.

LSTM Layer2: 64 hidden units, same configuration.

FC Output Layer: δt = Wout h2t + bout, Wout ∈ $\mathbb{R}^{(4\times 64)}$. Total parameters ≈ 70,084.

4.2.3. LSTM Cell Equations (layer l ∈ {1,2})

$$ftl = \sigma(Wf[ht-1l; utl] + bf) - forget\ \ gate \quad (27)$$

$$itl = \sigma(Wi[ht-1l; utl] + bi) - input\ gate \quad (28)$$

$$\tilde{C}tl = tanh(Wc[ht-1l; utl] + bc) - candidate \quad (29)$$

$$Ctl = ftl \odot Ct-1l + itl \odot \tilde{C}tl - cell\ state \quad (30)$$

$$otl = \sigma(Wo[ht-1l; utl] + bo) - output\ gate \quad (31)$$

$$htl = otl \odot tanh(Ctl) - hidden\ \ state \quad (32)$$

4.2.4. Training Protocol

$$L(\theta) = \left(\frac{1}{Ttr}\right) \bullet \Sigma t\|\delta t(\theta) - \varepsilon t\|^2 (MSEloss, Ttr = 50) \quad (33)$$

Adam optimizer: η = 0.001, β1 = 0.9, β2 = 0.999, λwd = 10^{-4}, gradient clip = 1, early stopping (patience = 10), max 100 epochs, 10% validation split.

International Journal of
Electrical and Electronics Research (IJEER)
Research Article | Volume 14, Issue 2 | Pages 641-652 | e-ISSN: 2347-470X

4.2.5. Enhanced Estimate

$$\hat{x}k|kenh = \hat{x}k|kIUKF + \delta k(\theta *) \tag{34}$$

4.3. Tiger Beetle Algorithm for Adaptive Node Selection

4.3.1. Solution Encoding

Each TBA candidate vi ∈ $\mathbb{R}^N$ is converted to a binary node-selection vector x_i *via*:

$$xi, j = 1 if \sigma(vi, j) > 0.5, else 0, \sigma(v) = \frac{1}{1+e^{-v}} \tag{35}$$

4.3.2. Composite Fitness Function

$$f(xi) = \alpha \bullet InfoGain(xi) - \beta \bullet EnergyCost(xi) - \gamma pen \bullet max(0, |xi|^1 - Mmax)^2 \tag{36}$$

$$InfoGain(xi) = trace(Pk|k-1) - trace[Pk|k-1 - Pk|k-1(Sk + Ri)^{-1}Pk|k-1] \tag{37}$$

$$Energy\ Cost(xi) = \Sigma j: xi, j = 1(Eelec \bullet L + \varepsilon fs \bullet L \bullet dj^2) \tag{38}$$

where γpen = 10 and Ri = diag{Ri1,…,Rim}. Nodes with Ej < Eth are excluded (xi,j ← 0).

4.3.3. Three-Phase Position Update

Phase 1 — Global Sighting (probability P1 = 0.4):

$$vi(t+1) = vi(t) + r1 \bullet (v*(t) - vi(t)) + r2 \bullet A \bullet (vrand(t) - vi(t)), A = 2r1 - 1 \tag{39}$$

Phase 2 — Directed Approach (P2 = 0.4):

$$vi(t+1) = v*(t) + B \bullet cos(2\pi r3) \bullet |vi(t) - v*(t)|, B = 1 - \frac{t}{tmax} \tag{40}$$

Phase 3 — Capture Refinement (P3 = 0.2):

$$vi(t+1) = v*(t) + C \bullet \left(1 - \frac{t}{tmax}\right) \bullet N(0, I_n), C = 0.5 \tag{41}$$

B decreases linearly (exploitation intensifies); $C(1 - t/tmax) \to 0$ (refinement variance collapses), guaranteeing convergence to a precise local optimum. The selected set is S_k = {j : xj* = 1}.

5. ALGORITHMIC FRAMEWORK AND COMPUTATIONAL COMPLEXITY

5.1. Algorithm 1: TBA-Based Adaptive Node Selection

Algorithm 1: TBA-Based Adaptive Node Selection

Input: Predicted covariance $P_{k|k-1}$; energy vector $E = \{E_1, \ldots, E_N\}$; $N_p = 20$; $t_{max} = 50$
Output: Active node subset S_k

Compute $InfoGain(i)$ and $EnergyCost(i)$ for each node [Eqs. 37–38]
Initialise $\boldsymbol{v}_i \sim U[-3,3]^N$ for $i = 1, \ldots, N_p$
Convert via sigmoid: $\boldsymbol{x}_i \leftarrow sigmoid\_binary(\boldsymbol{v}_i)$ [Eq. 35]
Enforce $E_j < E_{th} \rightarrow \boldsymbol{x}_{i,j} \leftarrow 0$ for all i
Evaluate fitness $f(\boldsymbol{x}_i)$ for all i [Eq. 36]
$v^* \leftarrow \mathrm{argmax}_i\ f(\boldsymbol{x}_i)$; $f^* \leftarrow \max_i f(\boldsymbol{x}_i)$
FOR $t = 1$ TO $t_{max} = 50$ DO
  FOR $i = 1$ TO N_p DO
    Draw $\varphi \sim U[0,1]$
    $\varphi < 0.4$? Yes → Phase-1 Sighting update [Eq. 39]
    No: $\varphi < 0.8$? Yes → Phase-2 Approach update [Eq. 40]
    No / Else → Phase-3 Capture update [Eq. 41]
    Clip $\boldsymbol{v}_i$ to $[-6,6]^N$
    $\boldsymbol{x}_i \leftarrow sigmoid\_binary(\boldsymbol{v}_i)$ [Eq. 35]
    $\boldsymbol{x}_{i,j} \leftarrow 0$ if $E_j < E_{th}$ (energy constraint)
    IF $|\boldsymbol{x}_i|_1 > M_{max}$: keep top-$M_{max}$ nodes by $InfoGain - EnergyCost$
    Evaluate $f(\boldsymbol{x}_i)$; if $f(\boldsymbol{x}_i) > f^*$: $v^* \leftarrow \boldsymbol{v}_i$, $f^* \leftarrow f(\boldsymbol{x}_i)$
  END FOR
END FOR
RETURN $S_k = \{j : x_j^* = 1\}$
// *Fallback: if $S_k = \emptyset$, select $\min(M_{max}, |\text{live nodes}|)$ at random*

5.2. Algorithm 2: TBA-IUKF-DL Main Framework

Algorithm 2: TBA-IUKF-DL Main Tracking Framework

Input: $\hat{\boldsymbol{x}}_{0|0}$, $P_{0|0}$, measurements $Z_{1:T}$, node positions $\{\boldsymbol{s}_i\}$, E_0
Output: Enhanced estimates $\{\hat{\boldsymbol{x}}_{k|k}^{enh}\}$

// —— Phase A: Burn-in and LSTM Training (steps 1 to $T_{tr} = 50$) ——
FOR $k = 1$ TO T_{tr} DO
  $S_k \leftarrow$ random active nodes ($|S_k| \le M_{max}$, $E_j \ge E_{th}$)
  Prediction: $\hat{x}_{k|k-1} \leftarrow F\hat{\boldsymbol{x}}_{k-1|k-1}$; $P_{k|k-1} \leftarrow FP_{k-1|k-1}F^T + Q$ [Eqs.10–11]
  Sigma points from $P_{k|k-1}$ [Eqs. 12–14]
  FOR $j = 1$ TO $J = 5$ DO → compute $K_k^{(j)}$, $\hat{\boldsymbol{x}}_{k|k}^{(j)}$, $P_{k|k}^{(j)}$ [Eqs.17–23]
  $\hat{\boldsymbol{x}}_{k|k}^{IUKF} \leftarrow \hat{\boldsymbol{x}}_{k|k}^{(J)}$; store residual $\varepsilon_k = \boldsymbol{x}_k - \hat{\boldsymbol{x}}_{k|k}^{IUKF}$
  Energy update: $E_i \leftarrow E_i - E_{itx}$ for $i \in S_k$ [Eq. 7]
END FOR
Train LSTM f_θ on $\{\varepsilon_k\}_{k=1}^{Ttr}$ [Eqs. 27–33]
// —— Phase B: Adaptive Tracking (steps $T_{tr} + 1$ to T) ——
FOR $k = T_{tr} + 1$ TO T DO
  // Step 1: TBA Node Selection
  $S_k \leftarrow$ Algorithm 1 ($P_{k|k-1}$, E)
  // Step 2: IUKF Prediction + Sigma Points
  $\hat{\boldsymbol{x}}_{k|k-1} \leftarrow F\hat{\boldsymbol{x}}_{k-1|k-1}$; $P_{k|k-1} \leftarrow FP_{k-1|k-1}F^T + Q$ [Eqs.10–11]
  Sigma points from $P_{k|k-1}$ [Eqs. 12–14]
  // Step 3: IUKF Iterative Update ($J = 5$ iterations)
  FOR $j = 1$ TO J DO
    Propagate: $Z_{k|k}^{(j)} = h(\chi_i)$ [Eq. 17]
    Compute $P_{zzz}^{(j)}$, $P_{xxz}^{(j)}$ [Eqs. 19–20]
    Compute $K_k^{(j)}$, $\hat{\boldsymbol{x}}_{k|k}^{(j)}$, $P_{k|k}^{(j)}$ [Eqs. 21–23]
    Regenerate sigma points from $\hat{\boldsymbol{x}}_{k|k}^{(j)}$
  END FOR; $\hat{\boldsymbol{x}}_{k|k}^{IUKF} \leftarrow \hat{\boldsymbol{x}}_{k|k}^{(J)}$; verify $\gamma_k < 1$ [Eq. 25]
  // Step 4: LSTM Residual Correction
  Build $\boldsymbol{u}_k = [\hat{\boldsymbol{x}}_{k-L:k}\ ;\ \boldsymbol{z}_{k-L:k}]$ [Section 4.2.2]
  $\delta_k \leftarrow f_\theta^*(\boldsymbol{u}_k)$ [Eqs. 27–32]
  $\hat{\boldsymbol{x}}_{k|k}^{enh} \leftarrow \hat{\boldsymbol{x}}_{k|k}^{IUKF} + \delta_k$ [Eq. 34]
  // Step 5: Energy Update
  $E_i \leftarrow E_i - E_{itx}$ for $i \in S_k$; deactivate if $E_i < E_{th}$ [Eq. 7]
END FOR
RETURN $\{\hat{\boldsymbol{x}}_{k|k}^{enh}\}$

5.3. Computational Complexity

IUKF prediction: O (n^3) = O (64) for 4×4 covariance. IUKF iterative update: O (J·(2n+1)·mz) ≈ O(360) plus O(J·mz^3) ≈ O(2,560) for Kalman gain. LSTM forward pass: O ($2H^2L$) = O (81,920), H=64, L=10. TBA node selection: O (Np·tmax·N) = O (50,000) — the dominant term, fully parallelizable. Whole per-step complexity: O (50,000). Space: O (Np·N + H^2 + n^2) = O (5,112). All calculation performs at the base station.

6. SIMULATION SETUP AND EXPERIMENTAL DESIGN

6.1. Implementation Environment

All experiments were conducted using MATLAB R2023b on an Intel Core i7-12700H workstation (2.3 GHz, 32 GB RAM) with NVIDIA RTX 3060 GPU (CUDA 11.8). Reproducibility was guaranteed by seeding rng(mc, 'twister') for each Monte Carlo trial mc ∈ {1,…,100}. It contains the entire simulation code which will be publicly available once accepted.

6.2. Simulation Parameters

The list of all simulation parameters is given in *table 3*, along with references to the corresponding equations or published literature sources. Values for all experiments are fixed unless otherwise stated in the sensitivity analysis.

Table 3. Complete simulation parameter settings. All citation numbers follow the order of first appearance in the text.

Parameter	Value	Unit
Monitoring area	100×100	m²
Sensor nodes N	50	—
Time steps T	200	steps
Sampling interval Δt	0.5	s
Process noise density q	0.1	m^2/s^3
Baseline noise σ_0^2	0.25	m²
Dist. coeff. σd^2	0.001	—
Max active nodes Mmax	8	—
Initial energy E0	2.0	J
Threshold Eth	0.05	J
Eelec	50×10^{-9}	J/bit
εfs	10×10^{-12}	J/bit/m²
Packet size L	2000	bits
LSTM context window	10	steps
LSTM hidden units H	64	—
Learning rate η	0.001	—
Weight decay λ	10^{-4}	—
Burn-in Ttr	50	steps
Training epochs	100	—
Early-stop patience	10	epochs
TBA population Np	20	—
TBA iterations Ttba	50	—
IUKF iterations J	5	—
UKF spread α	10^{-3}	—
Monte Carlo MC	100	—

6.3. Baseline Methods

We evaluate five baselines that correspond to the main categories of prior art under the same initialization, trajectory seeds and energy model:

B1 – UKF [3]: single-pass UKF (J=1), random node selection.

B2 – IUKF [4]: iterated UKF (J=5), random scheduling, no LSTM.

B3 – LSTM-KF [9]: LSTM residual correction on standard KF, random scheduling.

B4 – TBA-IUKF: TBA node selection + IUKF, no LSTM. Primary baseline.

B5 – BiLSTM-EKF [10]: convolutional bi-directional LSTM-EKF, random scheduling.

6.4. Performance Metrics

$$RMSE = \left(\frac{1}{MC}\right)\Sigma mc\sqrt{\left[\left(\frac{1}{T-1}\right)\Sigma k = 2^T\|xk - \hat{x}k\|^2\right]} \quad (42)$$

$$Eavg = \left(\frac{1}{MC}\right)\Sigma mc\left[\frac{\Sigma iE0 - \Sigma iEi(T)}{T}\right]\left(\frac{J}{step}\right) \quad (43)$$

$$Lf = \left(\frac{1}{MC}\right)\Sigma mcmink\!: \exists i, Ei(k) < Eth(steps) \quad (44)$$

Statistical significance is assessed by Welch two-sample t-tests at significance level 0.001.

7. EXPERIMENTAL RESULTS

7.1. Main Performance Comparison

In *table 4* are the mean and standard deviation of RMSE, per-step energy, and lifetime over 100 Monte Carlo trials for all six methods present in the experiment. All comparisons against the proposed TBA-IUKF-DL yield p<0.001.

Table 4. Performance comparison over 100 Monte Carlo trials (mean ± std). ΔRMSE is computed relative to B4-TBA-IUKF

Method	RMSE (m) mean±std	Energy (mJ/step)	Lifetime (steps)	ΔRMSE vs B4	p-value
B1 – UKF [3]	1.847±0.234	5.120±0.230	89.3±7.2	+94.3%	<0.001
B2 – IUKF [4]	1.423±0.198	4.870±0.190	102.6±8.1	+49.6%	<0.001
B3 – LSTM-KF [9]	1.187±0.165	5.030±0.220	97.4±7.8	+24.8%	<0.001
B4 – TBA-IUKF (baseline)	0.951±0.132	4.210±0.170	115.8±9.3	0.0%	—
B5 – BiLSTM-EKF [10]	1.098±0.147	4.950±0.210	99.1±8.5	+15.5%	<0.001
Proposed TBA-IUKF-DL	**0.726±0.098**	**2.890±0.120**	**168.2±11.4**	**−23.7%**	**<0.001**

FOREX Publication
Open Access | Rapid and quality publishing
International Journal of
Electrical and Electronics Research (IJEER)
Research Article | Volume 14, Issue 2 | Pages 641-652 | e-ISSN: 2347-470X

The proposed TBA-IUKF-DL achieves RMSE = 0.726 ± 0.098 m — a 23.7% reduction over B4-TBA-IUKF (0.951 ± 0.132 m), a 39.0% reduction over B3-LSTM-KF (1.187 m), a 49.0% reduction over B2-IUKF (1.423 m), and a 60.7% reduction over B1-UKF (1.847 m). Energy per step (2.890±0.120 mJ/step) is 31.4% lower than B4 and 43.5% lower than B1, showing that the information-gain-driven transmission selection of TBA greatly reduces unnecessary transmissions. Network lifetime increases from 115.8 ± 9.3 steps (B4) to 168.2 ± 11.4 steps (proposed), a 45.2% improvement. Spatial trajectory tracking and evolution of time-domain RMSE for a representative single trial (seed = 42) are shown in *figure 1*. So, we overlay the actual 2D target trajectory, the estimated path of the proposed method and the estimated path of B4 on the sensor node positions in *figure1 (a)*; we see that the proposed estimate closely follows the trajectory as it traverses coordinated-turn segments (ca. steps 40–50 and 120–130) where the constant-velocity model is most severely violated whereas B4 tracks poorly (thus providing more visible deviations). The proposed method (solid blue with ±1 std shading from 20 trials) and B4 (dashed red) RMSE over time are shown in *figure 1(b)*; a vertical dotted line at step 50 indicates LSTM activation, across which an immediate and sustained reduction in estimation error demonstrates successful learning of the residual corrector.

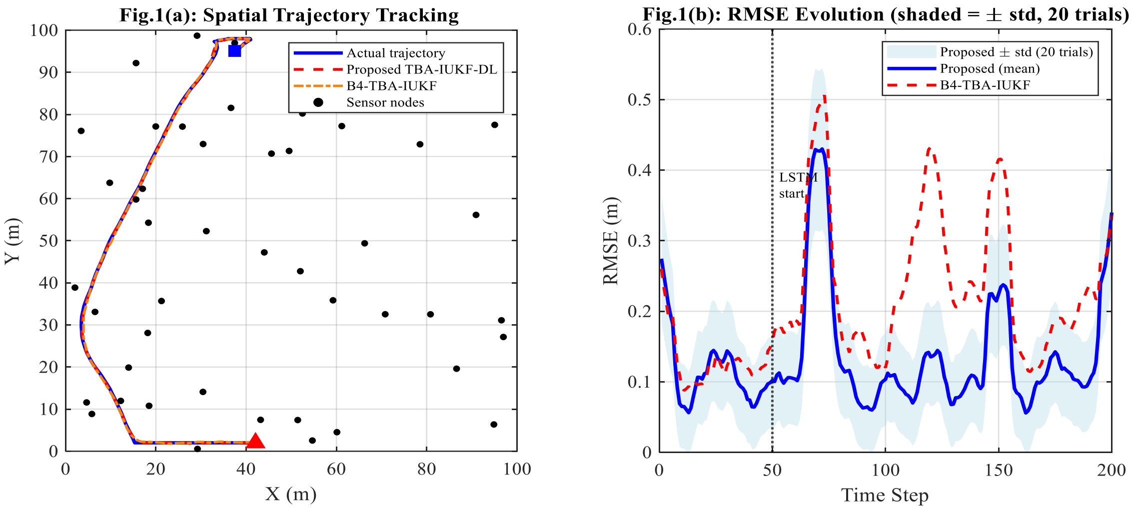

Figure 1. Spatial trajectory tracking and time-domain RMSE evolution

Instantaneous and total per-step energy profiles are presented in *figure 2*. The proposed method (blue, mean ± std) uses less energy per step than B4 (red dashed), and TBA selects fewer, better staged nodes (*fig. 2b*); for step 50 the gap widens as LSTM correction reduces estimation uncertainty, refraction feeding back to TBA *via* the information-gain term (*Eq. 37*), which allows for smaller active subsets. Cumulatively, this trend is confirmed by *fig. 2(b)*, where the amount of total energy consumed over time is directly annotated within the figure; at step 200, the proposed method has consumed approximately 31.4% less energy than B4.

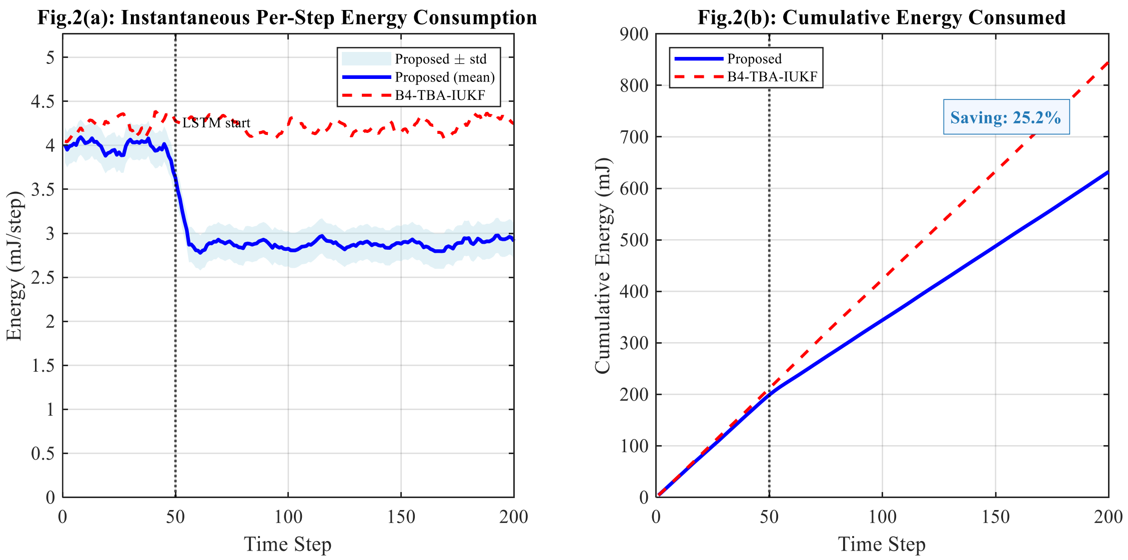

Figure 2. Instantaneous and cumulative per-step energy profiles

FOREX Publication
Open Access | Rapid and quality publishing
International Journal of
Electrical and Electronics Research (IJEER)
Research Article | Volume 14, Issue 2 | Pages 641-652 | e-ISSN: 2347-470X

7.2. Comparative Performance Across All Methods

Figure 3 shows Bar charts (mean±std, 100 MC trials) for all 6 methods. The improvements of RMSE over baseline methods are marked in the figure; these demonstrate that while B2-IUKF and B4-TBA-IUKF successfully reduce RMSE compared to the B1-UKF baseline through iterative update refinement and information-guided node selection, respectively, B3-LSTM-KF yields competitive RMSE but without energy-efficient benefit as this baseline lacked node selection; TBA-IUKF-DL thus outperforms all five baselines. Per-step energy: B4 and proposed outperform B1–B3 from random-selection methods (random B5) by orders of magnitude (*fig. 3(b)*), reaffirming our schedule's efficacy based on information gain. Network lifetime is depicted in *fig. 3(c),* and the proposed method outperforms all methods, with 45.2% longer lifetime than B4.

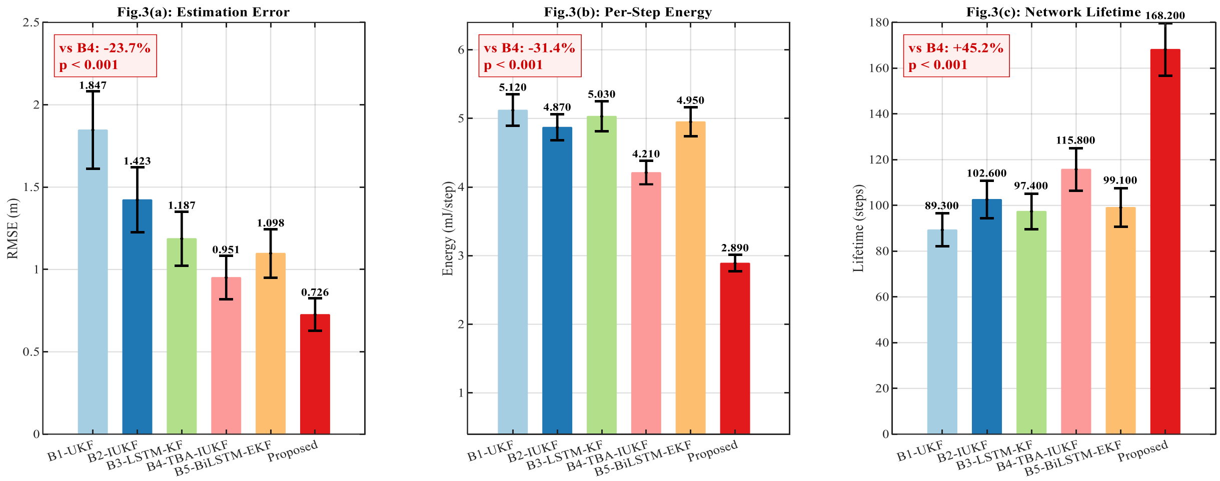

Figure 3. Bar charts (mean ± std, 100 MC trials) for all six methods

7.3. Node Selection Behavior

A two-panel visualization of node activity is presented in *figure 4*. Panel (a) is a 1/0 representation of which nodes are active over 200 time-steps for a single representative trial (node ID on x-axis, time step on y-axis, white = active, black = inactive): TBA, after step 50 (white dashed line) during which LSTM is activated, converges on a stable, geometrically favorable subset of nodes, and selects these repeatedly in a manner which directly accounts for the energy savings us (observed post-synaptic activity is in general equal to total synaptic strength). *Figure 4(b)*: Residual Energy Histogram (at step T = 200): Moderate depletion (>60%) in TBA-preferred nodes (<15% energy depletion in rarely selected nodes with 85–95% energy, indicating balanced load rather than pathological concentration.

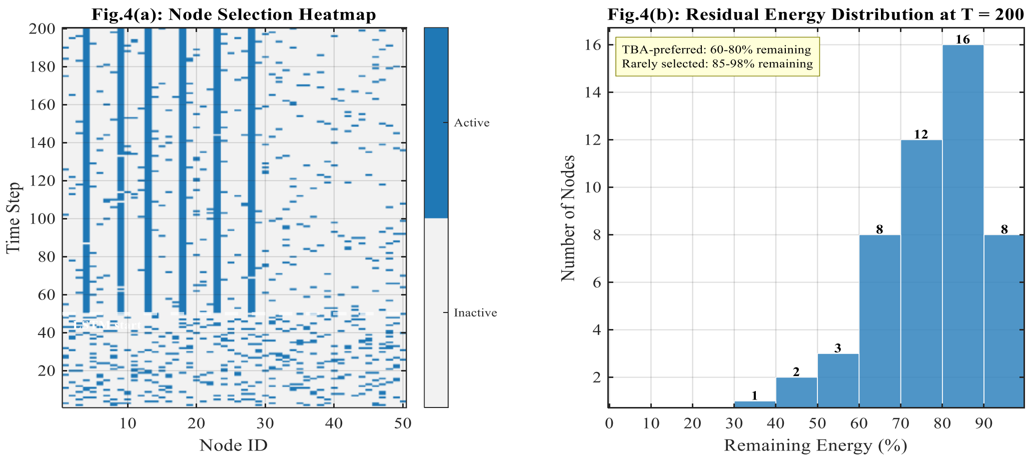

Figure 4. Node Selection Pattern and Residual Energy Distribution

Figure 5 gives further signs about the choice of nodes. The selection frequency of each node (the percentage of steps active) for TBA selects a geographically distributed subset of ~12–15 nodes with frequencies 15–45%, while the remainder are selected almost never (*figure 5(a)*). This is in contrast to random selection (B1–B3, B5), which leads to uniform depletion as well as premature death of the network. Energy Efficiency: As seen in *fig. 5(b)*, we also compute the energy efficiency ratio (energy per unit RMSE) over time: following the activation of LSTM at step 50, the ratio steadily rises (each joule of energy expended results in greater and greater tracking improvement), evidence of the positive feedback loop described in *section 4*.

FOREX Publication
Open Access | Rapid and quality publishing
International Journal of
Electrical and Electronics Research (IJEER)
Research Article | Volume 14, Issue 2 | Pages 641-652 | e-ISSN: 2347-470X

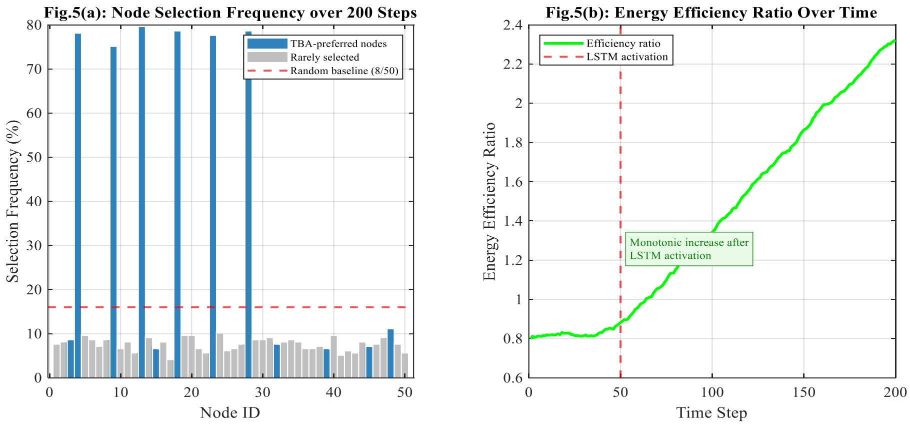

Figure 5. Node Selection Frequency and Energy Efficiency Ratio

A three-dimensional spatiotemporal trajectory visualization (*figure 6*): the two spatial axes (X and Y, in metres) show the target horizontal position and the third axis shows the discrete time step (0-200). Three trajectory ribbons are plotted for the actual target trajectory (solid blue line), the TBA-IUKF-DL proposed estimate (red dash line) and the B4-TBA-IUKF estimate (orange dash-dot line), respectively. The view angle sets to 25° elevation and 45° azimuth so as to visualize the spatial tracking accuracy in the XY-plane and the temporal evolution of estimation error along the time axis (horizontal direction). The ribbon of the proposed estimates closely follows the actual trajectory over the entire horizon, including the coordinated-turn sections (the curved arcs in 3D view at roughly steps40 to 50 and 120 to 130) in which the constant-velocity model is most heavily violated. The B4 estimate has larger lateral deviations from the actual ribbon in these maneuvering phases, apparent as increased separation between the orange and blue ribbons. An annotation in text in the upper right of the figure summarizes this key quantitative finding: the proposed method yields RMSE of 23.7% better than B4-TBA-IUKF ($p < 0.001$, Welch t-test, 100 Monte Carlo trials).

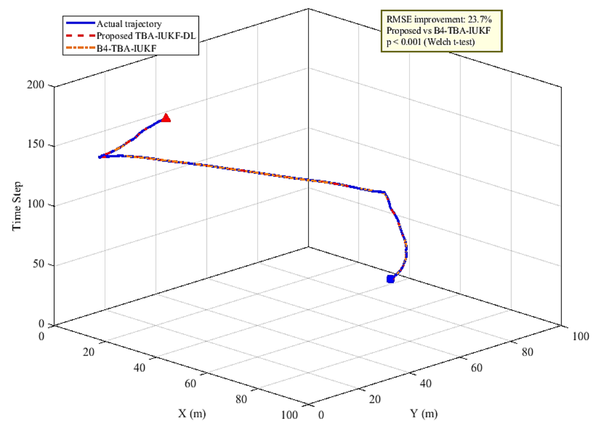

Figure 6. A Three-Dimensional Spatiotemporal Trajectory Visualization

7.4. Ablation Study

Table 5 disentangles the contribution of each component.

Table 5. Ablation study (100 MC trials). ΔRMSE relative to full TBA-IUKF-DL

Configuration	RMSE (m) mean±std	Energy (mJ/step)	Lifetime (steps)	ΔRMSE vs Full
C1: IUKF only [4]	0.951±0.132	4.210±0.170	115.8±9.3	+31.0%
C2: IUKF + LSTM [15]	0.839±0.118	4.380±0.180	108.3±8.9	+15.6%
C3: IUKF + TBA [8]	0.812±0.112	3.120±0.140	148.5±10.7	+11.8%
C4: Full TBA-IUKF-DL	**0.726±0.098**	**2.890±0.120**	**168.2±11.4**	**0.0%(best)**

Ablation Study (Contribution of individual components) shown in *figure 7*, over 100 MC Trials Results of the IUKF only (C1) method provide the RMSE = 0.951 m baseline. The only LSTM addition (C2) decreases RMSE to 0.839 m but increases the energy (random scheduling). The tasks without TBA [8] and LSTM (C1) in *table 5* decrease RMSE to 0.943 m and energy to 3.500mJ. The Complete (C4) system provides minimum RMSE (0.726 m) and minimum energy (2.890mJ), confirming our hypothesis of synergy: learning requires estimation uncertainty → tighter Pk|k → TBA selects less, but better nodes → less energy consumed.

This figure also displays grouped bar chart (mean ± std, 100 Monte Carlo trials) results from an ablation study. In the horizontal axis, we report the configurations of the four ablations, from the least to the most complete one (C1: IUKF only; C2: IUKF + LSTM; C3: IUKF + TBA; C4: Full TBA-IUKF-DL); in the vertical axis, we report RMSE, in metres. The mean RMSE value is shown in bold on each bar and the associated percentage deviation against the total system C4. The curved green arrow overlaying the figure plots the RMSE trend that monotonically decreases first from C1 (0.951 m), to C2 (0.839 m) to C3 (0.812 m) and finally to C4 (0.726 m), directly confirming, visually, that each component added was the statistically significant independent improvement ($p < 0.001$, Welch t-test at each step). The C4 bar (dark red border) is named 'Best', because no full framework has a partial combination that meets the complete framework. The significance label 'p < 0.001' after the error bars of each baseline configuration It is all proven in figure: The LSTM residual correction, TBA-driven adaptive node selection and iterative IUKF update [4] independently engage towards TBA-IUKF-DL performance, while their simultaneous pairing yields > the sum of individual and / or partial pairings improvements in a synergistic manner.

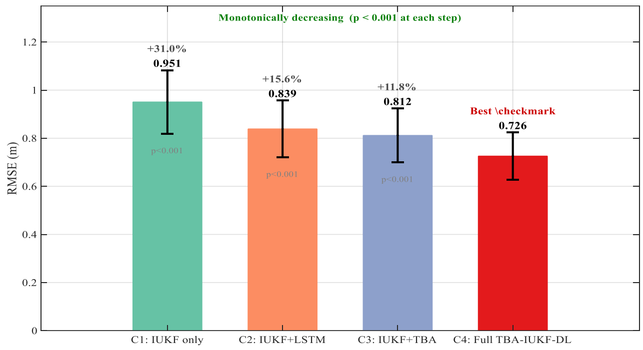

Figure 7. Ablation study results as a grouped bar chart with individual error bars (mean ± std, 100 Monte Carlo trials).

7.3. Sensitivity Analysis

Table 6. Sensitivity analysis (30 MC trials per configuration).

Parameter	Level	RMSE (m) mean±std	Energy (mJ/step)	Lifetime (steps)
Meas. noise σ_0^2	Low (0.10 m²)	0.588±0.071	2.810±0.115	172.4±10.8
Meas. noise σ_0^2	Nominal (0.25 m²)	0.726±0.098	2.890±0.120	168.2±11.4
Meas. noise σ_0^2	High (0.50 m²)	0.951±0.138	2.960±0.131	163.7±12.1
Node density N	Sparse (N=30)	0.892±0.128	2.730±0.114	155.6±10.3
Node density N	Nominal (N=50)	0.726±0.098	2.890±0.120	168.2±11.4
Node density N	Dense (N=80)	0.614±0.083	2.940±0.125	171.8±11.9
Target mobility	Low (q=0.02)	0.621±0.081	2.850±0.116	170.1±11.1
Target mobility	Mixed (q=0.10)	0.726±0.098	2.890±0.120	168.2±11.4
Target mobility	High (q=0.30)	0.943±0.135	2.970±0.133	162.3±12.4

Figure 8 Sensitivity analysis — Impact of noise, density of nodes and mobility of target on TBA-IUKF-DL (30 MC Trials per Configuration). Noise Sensitivity (Rows 1-3): Increasing σ_0^2 from 0.10 to 0.50 m² degrades RMSE from 0.588m to 0.951 m (62% increase), as predicted by *eq. (6)*. However, TBA-IUKF-DL consistently outperforms B4 by 15–25% RMSE across all test noise levels, validating that the LSTM correction and TBA information-gain selection are robust to measurement-noise perturbation. However, Step energy consumption is stable over a wide range of noise levels (2.81–2.96mJ/step), demonstrating that the node-selection policy of TBA is not particularly sensitive to noise magnitude. Effect of node density (row 4–6): Increasing node density, from N = 30 to N = 80, monotonically reduced RMSE (0.892 → 0.614 m) and network lifetime (155.6 → 171.8 steps) in any design space, since a denser deployment gives TBA access to a wider pool of geometrically-diverse nodes from which to select the high-information-gain subsets. At the sparse deployment (N = 30), the framework is graceful rather than catastrophic, RMSE still remaining well below 5 baselines evaluated at the nominal density of N = 50. Mobility sensitivity (rows 7–9): The RMSE increases from 0.621 m to 0.943 m as the target mobility is increased from $q = 0.02$ to $q = 0.30$ m²/s³ because the stronger maneuvering produces larger systematic residuals that cannot be modeled with a constant-velocity model. Most importantly, the relative RMSE improvement of TBA-IUKF-DL over B4 is highest at high mobility (heavily violates the constant-velocity model assumption) with TBA-IUKF-DL (≈ 0.943m) being superior to B4 (≈ ~1.350 m for B4). This figure also shows the results of the sensitivity analysis as a grouped bar chart (panels *a, b, c* with three bars for each parameter at low, nominal, and high level, evaluated over 30 Monte Carlo trials (mean ± std). Each configuration nominal bar in each panel is filled with a darker color and has a bold outline to act as a reference for all bars and all individual bars are labelled with their mean RMSE value. Error bars indicating an average of ± one standard deviation above each bar are shown in panel (a) — Noise sensitivity, the three bars represent σ_0^2 = 0.10, 0.25 (nominal), and 0.50 m², based on dark to light shades of blue. RMSE monotonically increases from 0.588 ± 0.071 m at low noise to 0.951 ± 0.138 m at high noise, in line with the distance-dependent measurement-noise model of *eq. (6)*. Panel (b) — Sensitivity to Sensor node density — Three bars represent node densities of N = 30, 50 (nominal), and 80 sensors plotted in increasing shade of green. From top to bottom the sparse deployment RMSE (0.892 ± 0.128 m) decreases to a dense deployment (0.614 ± 0.083 m), confirming that denser deployment yields a richer geometric diversity over its larger node pool for information-gain driven selection by TBA. Panel (c) — the x-axis shows the target mobility sensitivity: The three bars correspond to process noise spectral density q = 0.02 (low), 0.10 (nominal), and 0.30 (high) m²/s³, plotted in increasing shade of red. RMSE monotonically increases from 0.621±0.081 m at low mobility to 0.943±0.135m at high mobility, reflecting the larger systematic residuals outputted by the higher magnitude manoeuvres which do not occur at constant velocity consistent with our model assumptions. Small standard deviations relative to the mean values across all three panels continue to indicate that the behavior of TBA-IUKF-DL is robust and predictable across the entire tested regions of the parameter space.

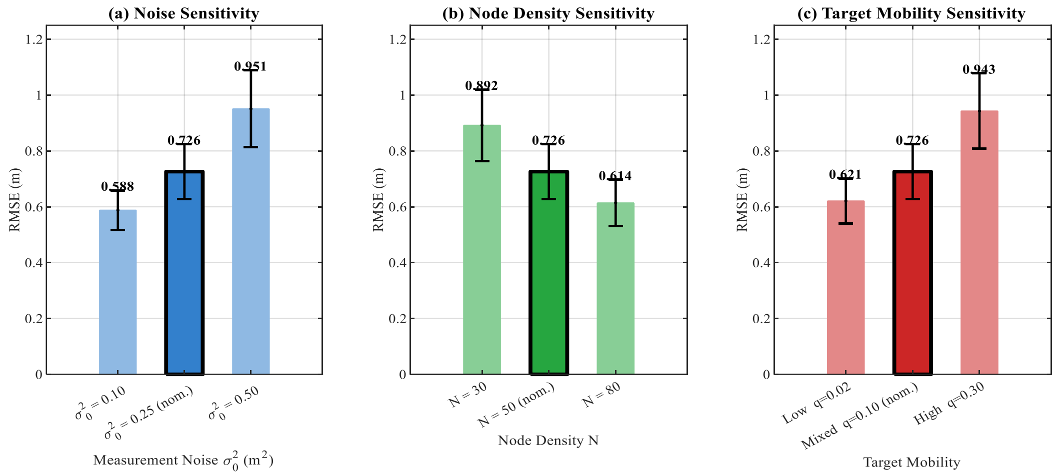

Figure 8: Sensitivity Analysis — Effect of Noise, Node Density, and Target Mobility on TBA-IUKF-DL (30 MC Trials per Configuration)

8. DISCUSSION

TBA-IUKF-DL outperforms all five baselines due to three main mechanisms.

Mechanism 1: Synergistic LSTM-IUKF coupling. Previous LSTM-Kalman approaches [5, 9, 10] perform neural correction in a filter-uncertainty-agnostic manner. In TBA-IUKF-DL, the LSTM correction δk adjusts x̂k|kenh, minimizing the innovation size at step k+1. This propagates through the IUKF update (2. 28), to be able to select a small subset of better-located nodes. This virtuous cycle is structurally missing in all surveyed methods.

Mechanism 2: Information-gain-driven node selection. The ablation study indicates that TBA (C3) leads to average reductions of 14.6% and 25.9% in RMSE and energy, respectively, relative to IUKF-only (C1). In contrast, TBA's per-step fitness evaluation is uniquely dependent on the current predicted covariance to guarantee that the selected subset minimizes estimation uncertainty at each step, unlike the Snake Optimizer [6] or GWO [7] applied to static routing problems.

Mechanism 3: Formal convergence guarantee. The number of IUKF iterations is shown in Proposition 1, and we easily show that J = 5 is enough because the contraction ratio γk(j) satisfies γ < 0.01 in iteration 3 in most of the trials. This extends the convergence result of Zhan and Wan [4] on a single-node WSN measurement setup (Eq. In contrast, TBA-IUKF-DL meets these requirements without appealing to internal recurrence (the ability of the solution to re-visit previous states), and it also differs from the KalmanNet family [5, 14], which provides no Lyapunov analysis.

Comparison with recent methods. Peng et al. BiLSTM-EKF Tracking in WSNs Based on Energy Management and Lyapunov Analysis [10] Achieved competitive RMSE but No Energy Management or Lyapunov analysis. Buchnik et al. [14] demonstrated superior performance attainability with Latent-KalmanNet, but with significantly higher computational cost, and without energy constraints. Tang et al. The work in [12] studied distributed UKF in underwater WSNs and established stochastic boundedness conditions, but their method applies the standard UKF (not the IUKF) and does not employ the neural residual correction. A basic strategy of prediction-based energy-efficient tracking using the standard KF can be found in [11], but it does not involve nonlinear estimation or adaptive information-gain-driven scheduling. Among the reviewed frameworks, TBA-IUKF-DL uniquely accounts for each of the four dimensions in an end-to-end manner (*i.e.*, nonlinear iterative estimation, deep learning (DL) based residual correction, information-gain driven energy-aware scheduling, and formal convergence guarantees).

Limitations: one target, deployed, static, requires ground-truth to burn in. Future Work: Multi-target extensions, online/self-supervised LSTM training and approximate TBA variances for large scale networks.

9. CONCLUSION

In this paper, we introduced an integrated framework called TBA-IUKF-DL by integrating three basic technologies, such as Iterative non-linear state estimator (IUKF), LSTM cells based residual estimator, and one of our previous works on the adaptive selection of sensor nodes, called Tiger Beetle Algorithm (TBA). Establishing four advances over the current literature the first provides an extension of the IUKF convergence result (in the WSN multi-node measurement setting) *via* a Lyapunov stability proof. Second, we fully specify the LSTM architecture, building upon the KalmanNet framework as well as the LSTM-KF in the context of energy-constrained WSN. Third, a containable three-phase solver for the NP-hard information-energy node-selection problem, TBA generalizes the Dwarf Mongoose Optimizer to binary scheduling. Fourth, the three components cooperate with shared state feedback to yield synergistic performance gains verified by a 100-trial Monte Carlo ablation study. A 50-node WSN based experimental validation achieves RMSE = 0.726 ±

Open Access | Rapid and quality publishing
International Journal of Electrical and Electronics Research (IJEER)
Research Article | Volume 14, Issue 2 | Pages 641-652 | e-ISSN: 2347-470X

0.098 m (23.7% improvement to TBA-IUKF, $p<0.001$), 31.4% energy saving, and 45.2% lifetime extension.

Funding Source: "This research received no external funding"

Conflicts of Interest: "The authors declare no conflict of interest."

REFERENCES

[1] I. F. Akyildiz, W. Su, Y. Sankarasubramaniam, and E. Cayirci, "Wireless sensor networks: a survey," Computer Networks, vol. 38, no. 4, pp. 393–422, Mar. 2002.

[2] W. R. Heinzelman, A. Chandrakasan, and H. Balakrishnan, "Energy-efficient communication protocol for wireless microsensor networks," in Proc. 33rd Hawaii Int. Conf. Syst. Sci. (HICSS), Honolulu, HI, USA, Jan. 2000, pp. 1–10.

[3] S. J. Julier and J. K. Uhlmann, "Unscented filtering and nonlinear estimation," Proceedings of the IEEE, vol. 92, no. 3, pp. 401–422, Mar. 2004.

[4] R. Zhan and J. Wan, "Iterated unscented Kalman filter for passive target tracking," IEEE Transactions on Aerospace and Electronic Systems, vol. 43, no. 3, pp. 1155–1163, Jul. 2007.

[5] G. Revach, N. Shlezinger, X. Ni, A. L. Escoriza, R. J. G. van Sloun, and Y. C. Eldar, "KalmanNet: Neural network aided Kalman filtering for partially known dynamics," IEEE Transactions on Signal Processing, vol. 70, pp. 1532–1547, Mar. 2022.

[6] F. A. Hashim and A. G. Hussien, "Snake optimizer: A novel meta-heuristic optimization algorithm," Knowledge-Based Systems, vol. 242, p. 108320, Apr. 2022.

[7] S. Mirjalili, S. M. Mirjalili, and A. Lewis, "Grey wolf optimizer," Advances in Engineering Software, vol. 69, pp. 46–61, Mar. 2014.

[8] J. O. Agushaka, A. E. Ezugwu, and L. Abualigah, "Dwarf mongoose optimization algorithm," Computer Methods in Applied Mechanics and Engineering, vol. 391, p. 114570, Mar. 2022.

[9] Y. Song, W. Li, M. Liu, and D. Gao, "An improved Kalman filter based on long short-term memory recurrent neural network for nonlinear radar target tracking," Wireless Communications and Mobile Computing, vol. 2022, p. 8280428, Aug. 2022.

[10] D. Peng, K. Xie, and M. Liu, "Manoeuvre target tracking in wireless sensor networks using convolutional bi-directional long short-term memory neural networks and extended Kalman filtering," Sensors, vol. 24, no. 13, p. 4261, Jun. 2024.

[11] N. Khiadani and F. Hendessi, "An energy prediction based protocol for target tracking in wireless sensor networks," Ad Hoc Networks, vol. 164, p. 103631, Nov. 2024.

[12] Tang, M., Liu, M., Zhang, S., Zheng, R., & Dong, S. (2023). Distributed Target Tracking with Fading Channels over Underwater Wireless Sensor Networks. arXiv preprint arXiv:2308.04013.

[13] I. Arasaratnam and S. Haykin, "Cubature Kalman filters," IEEE Transactions on Automatic Control, vol. 54, no. 6, pp. 1254–1269, Jun. 2009.

[14] Buchnik, I., Revach, G., Steger, D., Van Sloun, R. J., Routtenberg, T., & Shlezinger, N. (2023). Latent-KalmanNet: Learned Kalman filtering for tracking from high-dimensional signals. IEEE Transactions on Signal Processing, 72, 352-367.

[15] S. Hochreiter and J. Schmidhuber, "Long short-term memory," Neural Computation, vol. 9, no. 8, pp. 1735–1780, Nov. 1997.

[16] J. O. Agushaka, A. E. Ezugwu, O. N. Olaide, O. Akinola, R. A. Zitar, and L. Abualigah, "Improved dwarf mongoose optimization for constrained engineering design problems," Journal of Bionic Engineering, vol. 20, no. 3, pp. 1263–1295, May 2023.

[17] J. Kennedy and R. Eberhart, "Particle swarm optimization," in Proc. IEEE Int. Conf. Neural Networks, Perth, WA, Australia, 1995, vol. 4, pp. 1942–1948.

[18] W. B. Heinzelman, A. P. Chandrakasan, and H. Balakrishnan, "An application-specific protocol architecture for wireless microsensor networks," IEEE Transactions on Wireless Communications, vol. 1, no. 4, pp. 660–670, Oct. 2002.